



CHORUS

This is the accepted manuscript made available via CHORUS. The article has been published as:

Time dependence of fast electron beam divergence in ultraintense laser-plasma interactions

K. U. Akli, M. J. Storm, M. McMahon, S. Jiang, V. Ovchinnikov, D. W. Schumacher, R. R. Freeman, G. Dyer, and T. Ditmire

Phys. Rev. E **86**, 026404 — Published 14 August 2012

DOI: [10.1103/PhysRevE.86.026404](https://doi.org/10.1103/PhysRevE.86.026404)

The Time-dependence Of Fast Electron Beam Divergence In Ultra-intense Laser-Plasma Interactions

K. U. Akli, M. J. Storm, M. McMahon, S. Jiang, V. Ovchinnikov, D. W. Schumacher, R. R. Freeman
The Ohio State University, Columbus, Ohio 43210, USA

G. Dyer, T. Ditmire
University of Texas at Austin, Austin, Texas 78712, USA

We report on the measurement and computer simulation of the divergence of fast electrons generated in an ultra-intense laser-plasma interaction (LPI) and the subsequent propagation in a non-refluxing target. We show that, at $I\lambda^2$ of 10^{20} Wcm⁻²μm², the time-integrated electron beam full divergence angle is $(60 \pm 5)^\circ$. However, our time-resolved 2D PIC simulations show the initial beam divergence to be much smaller ($\leq 30^\circ$). Our simulations show the divergence to monotonically increase with time, reaching a final value of $(68 \pm 7)^\circ$ after the passage of the laser pulse, consistent with the experimental time-integrated measurements. By revealing the time dependent nature of the LPI, we find that a substantial fraction of the laser energy ($\sim 7\%$) is transported up to 100 μm with a divergence of 32° .

PACS numbers: 52.38.-r, 52.50.Jm

I. INTRODUCTION

The interaction of an ultra-intense laser with solid targets—the so called LPI (*laser-plasma interaction*)— is of great interest to many applications, including isochoric heating of matter [1–3], proton and heavy ion acceleration [4–6], bright X-ray sources [7], and electron-positron pair production [8]. Advancing and optimizing these applications requires understanding the physics of the generation of the fast electrons by ultra-intense lasers and their subsequent transport in solid density matter.

There are many experimental factors that affect the general characteristics of the LPI; electron beam source size, mean energy, energy distribution, and divergence. These include the laser pulse profile, target material, and combinations of the two. Most ultra-intense lasers have an inherent amplified spontaneous stimulated emission (ASE) pedestal that precedes the main pulse on a nanoseconds scale. This pedestal is often intense enough to pre-ionize the target creating a pre-formed plasma with which the main pulse interacts. This pre-formed plasma is known to affect both the laser pulse propagation and the electron beam generation [9]. Although the preformed plasmas can hinder some applications such as fast ignition [10], it is desirable in many others. For example long scale pre-formed plasmas generate an extremely energetic tail in the electron energy distribution that can benefit laser wake field acceleration, bright X-ray sources, and electron-positron pair production.

The laser-generated electron beam divergence angle has recently received a lot of attention in laser-plasma interaction experiments. Various techniques have been used to measure this parameter: e.g., K_α fluorescence measurements [11, 12], Coherent Transition Radiation (CTR) [13], and Planckian emission imaging [14]. The published full angle values for the beam divergence range from 30° to as much as 100° . One of the reasons for the discrepancy in the reported values is that experiments

are carried out with thin targets where the electron trapping and circulation, due to the electrostatic sheath that forms around the target, complicates the data interpretation [15, 16].

There is a developing consensus in the high energy density physics community that the ultra-intense laser generated electron beam divergence angle is larger than can be tolerated for some applications such as fast ignition, consistent with the measurements of Green et al. (2008). However, this conclusion is based on time-integrated measurements and only applies to the final beam divergence. Here we argue that it is meaningless to talk about a single beam divergence value since the measurements are affected by time-dependent local magnetic fields and target surface electric fields which also vary in time. In many, if not most applications, the useful figure of merit is not the time-integrated beam divergence angle, but rather the spatial spread of the fast electrons as a function of time, and the distribution of energy they represent at a given time. For example: How do the electron beam flux and energy transport evolve with time? Do these quantities significantly change before and after the laser pulse is off?

In this paper, we report on electron beam divergence measurements using non-relaxing targets. We use the PIC code LSP to model these massive targets to get insight into the time-dependent behavior of electron beam divergence and energy transport. In what we believe to be a first, the simulations include not only a full laser-plasma interaction (LPI) with spatial and time resolution sufficient to represent all of the relevant dynamics, but the subsequent transport of the fast electrons, including dynamic ionization, and electron scattering, throughout an extended target.

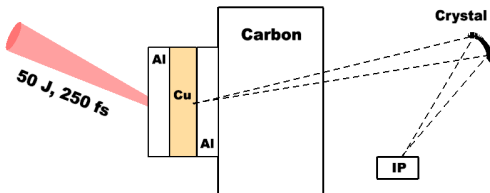


FIG. 1. (Color online) Experimental setup: 50 J 250 fs laser beam incident on Al/Cu/Al/C target. The K_{α} photons induced by electrons in Cu are collected using a spherically bent Bragg crystal

II. EXPERIMENTAL SETUP AND RESULTS

The experiments were conducted on the Texas Petawatt laser system at the University of Texas at Austin. The laser delivered 50J of energy at a wavelength of $1.054 \mu\text{m}$. The pulse length, measured with a second order autocorrelator, was 250 fs full width at half maximum intensity (FWHM). The laser beam was focused with an $f/3$ off-axis parabola and the intensity distribution was determined by imaging the focal spot at low power. The peak laser intensity was $1.2 \times 10^{20} \text{ Wcm}^{-2}$ with 50% of the energy focused in excess of $2.5 \times 10^{19} \text{ Wcm}^{-2}$. The pre-pulse was not monitored during this experiment. However, the preformed plasma scale length was about $1.5 \mu\text{m}$, indirectly determined from the sensitivity of the K_{α} images to pre-pulses [16], as discussed in Section III. The laser beam irradiated the Al/Cu/Al/C targets at 30° angle of incidence. The thickness of the Al layer in front of the $25 \mu\text{m}$ Cu tracer layer was either $15 \mu\text{m}$, $50 \mu\text{m}$, or $100 \mu\text{m}$. The Al layer behind Cu was $20 \mu\text{m}$ thick. To minimize rear and side electron refluxing a large carbon layer was fixed to the rear side of the target to act as a fast electron absorber. This layer was 1 mm thick and $5 \text{ mm} \times 10 \text{ mm}$ in the transverse direction.

The K_{α} photons induced by electrons in Cu were collected using a spherically bent Bragg Quartz crystal [17]. The photons were then detected with BAS-MS 2040 imaging plates and scanned with a Fuji FLA7000 scanner to obtain 2D spatially resolved images of the target. Fig. 2-a shows typical experimental data along with the horizontal lineout. The two-dimensional image in the figure is a time-integrated spatial distribution of K_{α} emission induced in the Cu layer by laser-generated electrons. The horizontal lineout is averaged over 10 pixels and shows an emission spot of $80 \mu\text{m}$ full width at half intensity.

The time-integrated electron beam divergence angle is determined from K_{α} emission radii at various depths. Fig. 2-b is a plot of the K_{α} radius as a function of the Cu layer depth. Each data point represents the radius averages over a few shots with the error bars reflecting the standard deviation. A linear fit to this set of data is found using a weighted least square fit. The time-integrated

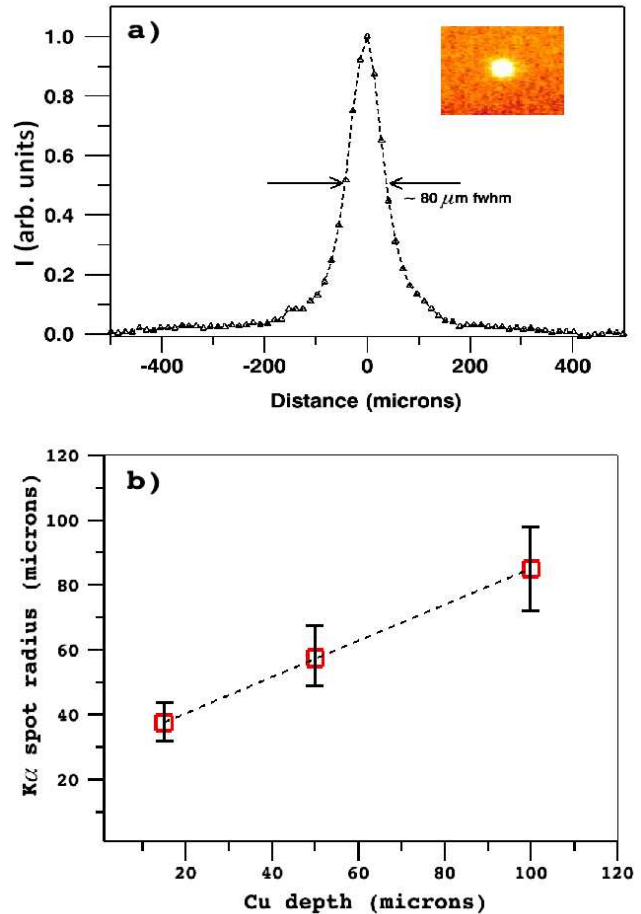


FIG. 2. (Color online) a) Typical experimental data: A K_{α} image with Cu tracer at a depth of $15 \mu\text{m}$ (inset); A horizontal lineout of the image showing an $80 \mu\text{m}$ spot size full width at half intensity. b) Experimental K_{α} radius as a function of Cu depth. Full divergence angle of $(60 \pm 5)^{\circ}$ is determined by weighted least square fit

electron beam divergence was determined from the slope of the linear fit to be $(60 \pm 5)^{\circ}$ full cone angle. This divergence angle is consistent with the values of $(58 \pm 7)^{\circ}$ and $(70 \pm 13)^{\circ}$ reported by Green et al. at laser intensities of $1.5 \times 10^{19} \text{ Wcm}^{-2}$ and $4 \times 10^{19} \text{ Wcm}^{-2}$ respectively [12].

III. 2D HYBRID-PIC SIMULATIONS: TIME-DEPENDENCE OF FAST ELECTRON BEAM DIVERGENCE AND FLUX

To reveal the time-dependence of the electron beam transport during and after the laser pulse, we have carried out full scale 2D implicit PIC simulations using LSP [18]. The $1 \mu\text{m}$ wavelength laser pulse was modeled as a sine-square function in time with a 250 fs FWHM. The 50J laser pulse spatial profile was modeled as a gaus-

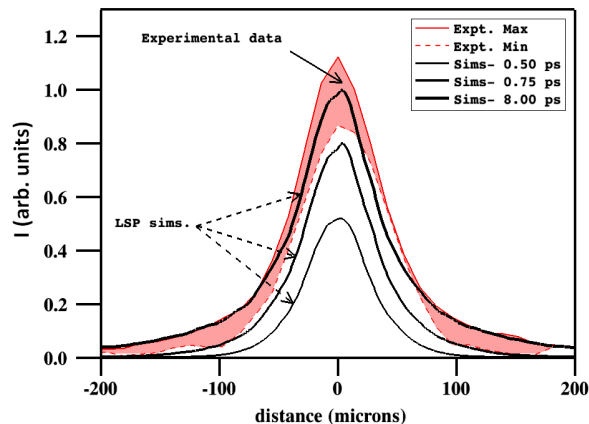


FIG. 3. (Color online) Time evolution of K_α emission at a depth of $15 \mu\text{m}$. The red band represents the range of the time-integrated experimental data. Black curves are the K_α profiles obtained from simulations at 0.50, 0.75, and 8.00 ps from bottom to top respectively

sian with $15 \mu\text{m}$ FWHM. The simulations were carried out in XZ cartesian geometry with the laser propagating in the X-direction. After propagating through a $40 \mu\text{m}$ vacuum region, the laser enters a low density pre-plasma region with a $1.5 \mu\text{m}$ scale length. The interaction of the laser with the pre-plasma takes into account dynamic ionization using the Ammosov-Delone-Krainov (ADK) model [19]. Segmented ionization through all ionization states was modeled on every time step. The spatial resolution starts at $\lambda/8 \times \lambda/8$ in the LPI region and linearly increases to $\lambda \times \lambda$ over $50 \mu\text{m}$ in the X-direction, remaining constant thereafter. The region adjacent to the pre-plasma had an initial solid density, was initially singly ionized, and a temperature of 5 eV. Electron scattering was treated using the Lee-More-Desjarlias collision model [20]. The carbon layer was modeled as a sink of electrons, as intended in the experiment, using the “conductor” model in LSP.

K_α emission induced by electron impact ionization was modeled by the Integrated Tiger Series (ITS) [21] code implemented in LSP. Five different depths (0, 15, 50, 75, and $100 \mu\text{m}$) were taken as K_α extraction planes. The experimental K_α images were first used to determine the pre-plasma profile scale length in the vicinity of the critical surface following the technique we recently introduced [16]. Briefly, the scale length was used as a single fitting parameter to match the K_α image profiles at all target depths. As explained in our previous work, images at different depths, and different regions of the same image at a given depth, have varying dependence to changes in scale length making this a sensitive technique. For this work, we found a pre-plasma scale length of $(1.5 \pm 0.3) \mu\text{m}$.

Fig. 3 shows the time evolution of the simulated K_α emission at a depth $15 \mu\text{m}$. The black curves labeled (1)

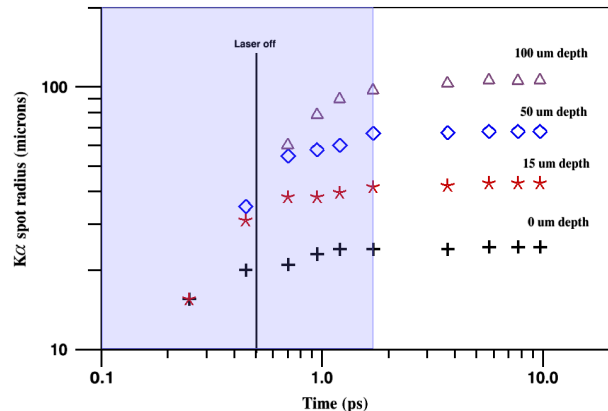


FIG. 4. (Color online) Time evolution of K_α spot size at 0, 15, 50, and $100 \mu\text{m}$ depths. The shaded area, the region of monotonically increasing K_α spot size. In the non-shaded area, the spot size becomes constant.

and (2) are the K_α profiles obtained from simulations at 0.50 and 0.75 ps respectively. Curve (3), the simulated profile after 8.00 ps, is in good agreement with the time-integrated experimental data range indicated by the red band. The time-dependent behavior of K_α emission at various depths is shown in Fig. 4. It is clear that the spot size increases with time and continues to increase even after the laser pulse is off. The rate at which the spot size increases is greater in the deeper planes as the most energetic electrons arrive there first. Closer to the laser-target interaction region, the growth rate is less as both fast and slow electrons contribute to the emission. More-

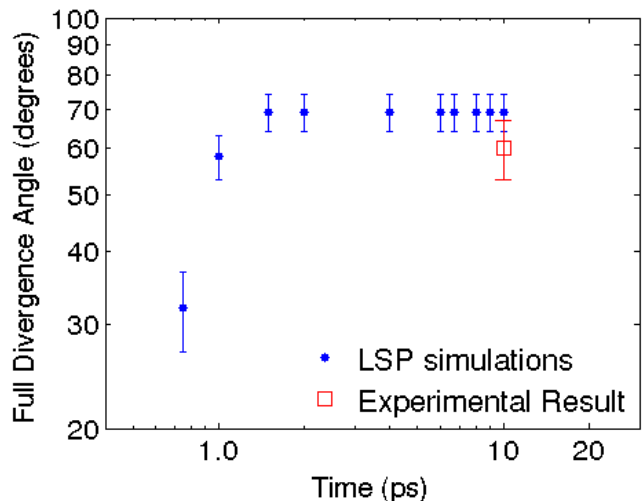


FIG. 5. (Color online) Time-dependent beam divergence from LSP simulations (blue), Time-integrated experimental measurement (red).

TABLE I. Time dependent divergence and cumulative flux at various depths due to all laser generated electrons with energies in excess of 9 keV.

Time (ps)	full div. angle (degrees)	Flux at 15 μm ($W\text{cm}^{-2}$)	Flux at 50 μm ($W\text{cm}^{-2}$)	Flux at 100 μm ($W\text{cm}^{-2}$)
0.75	32°	1.50×10^{20}	1.38×10^{20}	3.10×10^{19}
1.00	58°	1.92×10^{19}	2.29×10^{19}	2.98×10^{19}
1.50	69°	4.60×10^{18}	3.84×10^{18}	5.00×10^{18}
2.00	69°	2.56×10^{18}	1.63×10^{18}	1.10×10^{18}
4.00	69°	1.21×10^{17}	1.89×10^{17}	4.59×10^{16}

over, this rate is also affected by electrons that reflux from the front surface electrostatic sheath and return to the target where they contribute to the K_α emission. The increase in the K_α spot radius is followed by a plateau region which starts at about 1.7 ps and is depth independent. At any given time, the electron beam divergence is determined from the slope of the linear fit to the K_α spot radii at various depths. The time-dependent divergence is plotted in Fig. 5. It is clear that the initial beam divergence is small. This divergence increases monotonically with time and reaches a plateau in less than 2 ps. The final beam divergence is $(68 \pm 7)^\circ$, consistent with the time integrated experimental measurements.

To determine, the time dependent energy transport at various depths in the target, we use the K_α spot size and the corresponding electrons that induced the emission. At a given depth and given time, we first determine the K_α emission distribution in space. The full width at half maximum of the profile is then taken as a measure of the spot size. With this information and after computing the electron energy distribution that induced the emission, the time dependent electron beam flux is determined. The relationship between the fluxes at the three emission depths from the experiment and the beam divergence are shown in Table I. As the electron beam evolves with time, the flux decreases. For the 32° beam divergence angle, the fluxes at depths of 50 and 100 μm are 92% and 21% that of 15 μm respectively. In the calculation, we have included all electrons above 9 keV. The electron energy spectrum throughout the target has two populations; a hot population that can be described with a Boltzmann distribution and lower energy population. The hot tail of the distribution has a temperature of 7 MeV consistent with the ponderomotive scaling [22]. The laser-to-electron conversion efficiency in our experiment is determined by our simulations to be $\sim 45\%$, similar to the value reported by Yasuike et al. (2001) at $3 \times 10^{20} W\text{cm}^{-2}$ laser intensity [23].

Of current interest is the transport of the hot electron population, especially electrons with energy above 1 MeV that can carry energy deep into the target due to their long mean free path. We have looked at the transport of these electrons as they pass through an extraction plane as a function of time. We found that, the energy in elec-

trons above 1 MeV, transported within a 32° divergence angle, is 27%, 15 %, and 7% of the laser energy at depths of 15 μm , 50 μm , and 100 μm respectively. As a result of this initial narrow divergence, as much as 3.5 J of energy is transported to a depth of 100 μm by electrons with energies above 1 MeV.

IV. CONCLUSION

In conclusion, we have carried out experiments to study laser-generated electron beam divergence and energy transport at $I\lambda^2$ of $10^{20} W\text{cm}^{-2}\mu\text{m}^2$. We used targets with a Cu tracer and a large carbon layer to reduce or eliminate electron refluxing from the rear and side surfaces of the target. Our data shows that the time integrated electron beam divergence is wide $((60 \pm 5)^\circ)$, consistent with the most recent published results. However, by using our experimental data to benchmark our modeling, we showed that the initial beam divergence is narrower. We have asserted that it is meaningless to attach a single divergence value to the electron beam in laser plasma interactions due time-dependence. A substantial fraction of energy is transported up to 100 μm with a divergence of 32°. Our current results hold for low pre-pulse levels. Our simulations show that, at a constant laser intensity, an increase of pre-pulse level results in an increase in beam divergence angle. As the amount of pre-pulse becomes larger, the laser propagation to the critical surface becomes increasingly complex due to instabilities such as filamentation. This will be highly dependent on the laser intensity, pulse duration, and f-number. More work is needed to characterize the time evolution of the electron divergence and energy transport as a function of these quantities.

ACKNOWLEDGMENTS

KA would like to acknowledge R. Stephens, E. Gaul, M. Donovan, M. Martinez, and Texas Petawatt Laser team for their support. This work was performed under the auspices of the U.S. Department of Energy (DOE) under Contract DE-AC52-07NA27344, and DOE, Na-

tional Nuclear Security Administration (NNSA) Grant DE-FC5208NA28512 and DEFG5209NA29547, awarded

to the Center for High Energy Density Science at The University of Texas at Austin.

-
- [1] K. U. Akli, S. B. Hansen, A. J. Kemp, R. R. Freeman, F. N. Beg, D. C. Clark, S. D. Chen, D. Hey, S. P. Hatchett, K. Highbarger, et al., *Phys. Rev. Lett.* **100**, 165002 (2008).
- [2] P. M. Nilson, W. Theobald, J. F. Myatt, C. Stoeckl, M. Storm, J. D. Zuegel, R. Betti, D. D. Meyerhofer, and T. C. Sangster, *Phys. Rev. E* **79**, 016406 (2009).
- [3] G. Gregori, S. B. Hansen, R. Clarke, R. Heathcote, M. H. Key, J. King, R. I. Klein, N. Izumi, A. J. Mackinnon, S. J. Moon, et al., *Contributions to Plasma Physics* **45**, 284 (2005).
- [4] R. A. Snavely, M. H. Key, S. P. Hatchett, T. E. Cowan, M. Roth, T. W. Phillips, M. A. Stoyer, E. A. Henry, T. C. Sangster, M. S. Singh, et al., *Phys. Rev. Lett.* **85** (2000).
- [5] A. Maksimchuk, S. Gu, K. Flippo, and D. Umstadter, *Phys. Rev. Lett.* **84**, 4108 (2000).
- [6] S. Hatchett, C. Brown, T. Cowan, E. Henry, J. Johnson, M. Key, J. Koch, A. B. Langdon, B. Lasinski, R. Lee, et al., *Phys. of Plasmas* **7**, 2076 (2000).
- [7] C. Reich, I. Uschmann, F. Ewald, S. Düsterer, A. Lübcke, H. Schwoerer, R. Sauerbrey, E. Förster, and P. Gibbon, *Phys. Rev. E* **68**, 056408 (2003).
- [8] H. Chen, S. C. Wilks, J. D. Bonlie, E. P. Liang, J. Myatt, D. F. Price, D. D. Meyerhofer, and P. Beiersdorfer, *Phys. Rev. Lett.* **102**, 105001 (2009).
- [9] A. G. MacPhee, L. Divol, A. J. Kemp, K. U. Akli, F. N. Beg, C. D. Chen, H. Chen, D. S. Hey, R. J. Fedosejevs, R. R. Freeman, et al., *Phys. Rev. Lett.* **104**, 055002 (2010).
- [10] M. Tabak, *Phys. Plasmas* **1**, 1626 (1994).
- [11] R. B. Stephens, R. A. Snavely, Y. Aglitskiy, F. Amiranoff, C. Andersen, D. Batani, S. D. Baton, T. Cowan, R. R. Freeman, T. Hall, et al., *Phys. Rev. E* **69**, 066414 (2004).
- [12] J. S. Green, V. M. Ovchinnikov, R. G. Evans, K. U. Akli, H. Azechi, F. N. Beg, C. Bellei, R. R. Freeman, H. Habara, R. Heathcote, et al., *Phys. Rev. Lett.* **100**, 015003 (2008).
- [13] M. Storm, A. A. Solodov, J. F. Myatt, D. D. Meyerhofer, C. Stoeckl, C. Mileham, R. Betti, P. M. Nilson, T. C. Sangster, W. Theobald, et al., *Phys. Rev. Lett.* **102**, 235004 (2009).
- [14] K. L. Lancaster, J. S. Green, D. S. Hey, K. U. Akli, J. R. Davies, R. J. Clarke, R. R. Freeman, H. Habara, M. H. Key, R. Kodama, et al., *Phys. Rev. Lett.* **98**, 125002 (2007).
- [15] A. J. Mackinnon, M. Borghesi, S. Hatchett, M. H. Key, P. K. Patel, H. Campbell, A. Schiavi, R. Snavely, S. C. Wilks, and O. Willi, *Phys. Rev. Lett.* **86**, 1769 (2001).
- [16] V. M. Ovchinnikov, D. W. Schumacher, G. E. Kemp, A. G. Krygier, L. D. V. Woerkom, K. U. Akli, R. R. Freeman, R. B. Stephens, and A. Link, *Physics of Plasmas* **18**, 112702 (pages 9) (2011).
- [17] K. U. Akli, M. H. Key, H. K. Chung, S. B. Hansen, R. R. Freeman, M. H. Chen, G. Gregori, S. Hatchett, D. Hey, N. Izumi, et al., *Phys. Plasmas* **14**, 023102 (2007).
- [18] D. R. Welch, D. V. Rose, R. E. Clark, T. C. Genoni, and T. P. Hughes, *Computer Physics Communications* **164**, 183 (2004).
- [19] M. V. Ammosov, N. B. Delone, and V. K. Krainov, *Sov. Phys. JETP* **64**, 1191 (1986).
- [20] M. Desjarlais, *Contributions to Plasma Physics* **41**, 267 (2001), ISSN 1521-3986.
- [21] J. Halbleib, R. Kensek, G. Valdez, S. Seltzer, and M. Berger, *Nuclear Science, IEEE Transactions on* **39**, 1025 (1992).
- [22] S. C. Wilks, W. L. Kruer, M. Tabak, and A. B. Langdon, *Phys. Rev. Lett.* **69**, 1383 (1992).
- [23] K. Yasuike, M. H. Key, S. P. Hatchett, R. A. Snavely, and K. B. Wharton, *Review of Scientific Instruments* **72**, 1236 (2001).